The Upper- and Lower-Frequency Cutoffs of Magnetospherically Reflected Whistlers

B. C. EDGAR

The Aerospace Corporation, Laboratory Operations, Los Angeles, California 90009

The upper-frequency cutoffs of magnetospherically reflected (MR) whistlers observed by the Ogo 1 and 3 satellites are explained in terms of trapping of the upper-frequency components above the cutoff by sharp density gradients across L shells. The lower-frequency cutoffs are interpreted in terms of wave guide attenuation and D region absorption of the atmospheric source energy and defocusing of the MR whistler energy in the magnetosphere.

INTRODUCTION

Of the many VLF phenomena observed by the broad band (0.3–12.5 kHz) receivers aboard the Ogo 1 and 3 satellites [*Smith and Angerami*, 1968] the magnetospherically reflected (MR) whistler remains one of the most intriguing forms of nonducted whistler propagation. The MR whistler differs from the familiar 'ducted' whistler in that its ray path and wave normal direction deviate from the direction of the earth's magnetic field. As an introductory example to the MR whistler, Figure 1*a* shows how MR whistlers are received by a satellite on the geomagnetic equator. A lightning source illuminates the lower ionosphere, exciting a continuum of nonducted ray paths (represented by paths A, B, and C) in a model magnetosphere free of any sharp electron density irregularities. The wave normals, indicated by arrows along the ray paths, lag behind the direction of the static magnetic field and approach a transverse position by the time the rays cross the geomagnetic equator. Over much of their lengths the ray paths are directed outward with respect to the direction of the earth's magnetic field.

Energy following paths corresponding to ray path A is the first to intersect the satellite position on the geomagnetic equator. Because of its short path length this energy manifests itself on a satellite frequency-time spectrogram (shown in Figure 1*b*) as trace A, with minimal dispersion. Starting at lower initial latitudes than ray path A, paths B and C cross the geomagnetic equator at altitudes below the altitude of the satellite and extend well into the southern hemisphere. If the effects of both ions and electrons are included in the magnetospheric density model, the calculated ray paths B and C will abruptly turn around or 'reflect,' as first predicted by *Kimura* [1966]. This phenomenon can occur whenever the wave frequency falls below the local hybrid resonance (LHR) frequency. *Kimura* [1966] showed that in this case the wave normal angle can pass through 90°, resulting in a nearly 180° reversal of the ray direction.

After undergoing reflections in the southern hemisphere, ray paths corresponding to path B intersect the satellite, resulting in trace B in Figure 1*b*. Path C crosses underneath the satellite location and reflects in the northern hemisphere before reaching the satellite; the corresponding energy is represented by trace C in Figure 1*b*. The multiplicity of ray paths of MR whistlers implies that there is much information about the magnetosphere stored in their spectral characteristics.

MR WHISTLER RAY PATHS

It is instructive to examine the predicted frequency dependence of the MR paths in the case of a smooth magnetosphere Figure 2*a* illustrates differences between the second-component ray paths for frequencies below, above, and at the nose frequency. A dashed curve shows the limit beyond which the LHR frequency falls below 4 kHz. For the 1.5-kHz case the local LHR frequency is always above 1.5 kHz along the ray path. The ray therefore tends to be directed outward from the magnetic field vector. Consequently, the ray paths for frequencies below the nose must start at low L values (or low latitudes) to reach the satellite location.

The ray path for 4 kHz tends to be more field-aligned than that for 1.5 kHz, and most of the travel time is in regions of the magnetosphere where the local LHR frequency is less than 4 kHz. For frequencies well above the nose, such as the 10-kHz case, the ray must propagate to very low altitudes where $f_{LHR} \geq 10$ kHz in order to reflect. The long path forces the wave normal to rotate very close to the resonance cone of the refractive index surface. The looping inward of the 10-kHz ray path is a result of the proximity of the wave normal to the resonance cone before turnaround. (For a detailed explanation of the wave normal behavior during turnaround, based on a Snell's law construction, see *Edgar* [1972].) The resultant frequency dependence of MR whistler ray paths produces a 10° spread in starting latitudes.

The formation of the MR nose (or frequency of minimum travel time) only partially results from the ray path dependence on frequency. From Figure 2*a* one can deduce that the total path length for the second component increases monotonically with frequency. But the time delay is proportional to the integral of the group ray refractive index over the path [*Helliwell*, 1965]. For frequencies well below the nose the group ray refractive index varies as $1/f^{1/2}$, which results in the characteristic 'Eckersleylike' low-frequency dispersion shown by each component in Figure 2*b*. For the upper frequencies the increasing path lengths will correspondingly produce long time delays and the flattening of the MR traces above the nose. Between these two frequency ranges of characteristically long time delay there is a frequency for which the time delay integral minimizes, and this results in the nose signature on the frequency-time delay spectrogram. (See *Edgar* [1972] for a numerical proof.) Thus from the relative dispersion of a particular frequency component of an MR whistler trace one can deduce the type of MR ray path that produced it.

From the previous discussion one can account for certain

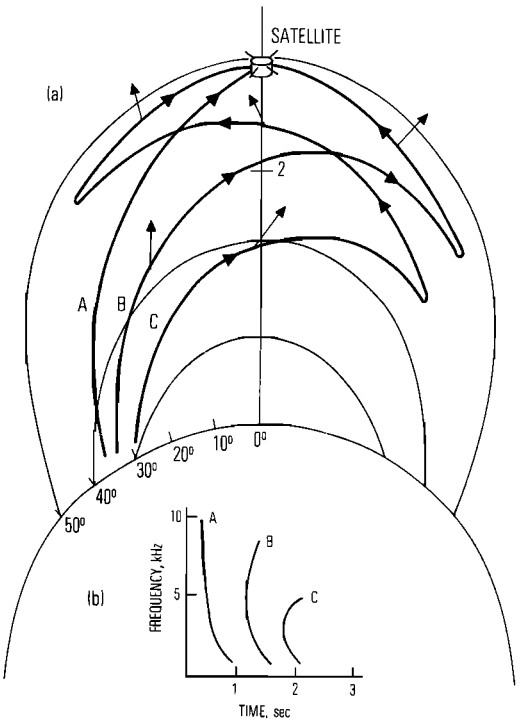

Fig. 1. (*a*) Ray paths for the first three components at 1.5 kHz of an MR whistler received at $L \sim 2.4$. The lightning source is located in the northern hemisphere. The wave normal direction is assumed to be vertical at the beginning of the path (500-km altitude) and is also shown at several points along the path. (*b*) The MR whistler frequency-time spectrogram corresponding to the ray paths in Figure 1*a*.

features of MR whistlers, i.e., the 'nose' characteristic dispersion of the traces and the time spacing between components on a spectrogram (see Figure 1*b*). *Smith and Angerami* [1968] took this approach in their qualitative explanation. However, this view of MR whistler observation by satellites cannot account for the upper- and lower-frequency cutoffs of observed MR whistlers. The purpose of this paper is to show how these upper- and lower-frequency cutoffs occur by means of propagational effects.

In the next sections this paper demonstrates quantitatively the strengths and weaknesses of 'smooth' magnetospheric models in predicting MR whistler frequency-time characteristics and gives a simple heuristic scheme for duplicating the cutoffs. Finally, it presents a magnetospheric electron density model which features a sharp cross-field density drop-off and which produces the observed frequency cutoff pattern on MR whistlers.

MR Whistler Spectra

Figure 3*a* shows a spectrogram of an MR whistler received on the Ogo 1 satellite near the geomagnetic equator at $L \sim 2.4$ on November 8, 1965. This example was chosen to illustrate the typical MR whistler cutoff structure and the complexities of interpretation. Of 461 MR multicomponent whistler events observed by Ogo 1 and 3 during 1965–1966 in the region bounded by $2.6 \leq L \leq 2.4$, 95% of the events exhibited some form of cutoff structure similar to the example of Figure 3*a*. Between $L \sim 2.2$ and $L \sim 2.4$, 63% of a total sample of 362 MR multicomponent whistler events exhibited a similar cutoff pattern. Above $L \sim 2.6$ all MR whistlers observed showed a cutoff structure.

The MR whistler of Figure 3*a* is characterized by six component traces spaced over a time interval of 4 s. The frequencies of minimum travel time or 'nose' frequencies range from ~4 kHz for the second component to ~2 kHz for the fifth component. The amplitudes of the traces are indicated by their relative darkness and width on the spectrogram photograph. Starting at 10 kHz the amplitude of the first trace increases with decreasing frequency until at ~1 kHz it undergoes a sharp cutoff. This cutoff results from the reaction of the satellite receiver automatic gain control (AGC) to the arrival of trace 2. The signal amplitudes of traces 1–4 were strong enough to cause the AGC to suppress the background noise. Thus the sharp lower-frequency cutoffs of traces 1, 2, and 3 and the upper-frequency cutoff of trace 3 are instrumental effects.

Regarding the relative amplitude of trace 4 as a function of increasing frequency the trace first appears above the background noise in Figure 3*a* at ~1 kHz and gradually increases in amplitude until the nose frequency is reached. We define gradual changes of amplitude as ones which occur smoothly over a 1-kHz or greater bandwidth and sharp or abrupt changes of amplitude as ones which occur in a 0.1-kHz-frequency bandwidth. Above the nose frequency the trace amplitude appears to remain at a constant level up to the 4-kHz upper cutoff. The enhanced amplitudes above 3 kHz on trace 4 also appear to cause the AGC to suppress the weaker portions of the trace below 3 kHz. Traces 5 and 6 exhibit sharp upper cutoffs similar to the cutoff of trace 4 but appear not to have AGC suppression of their lower-frequency (below the nose) portions. Thus the upper cutoffs of traces 4, 5, and 6 and the lower cutoffs of traces 5 and 6 appear to be natural phenomena.

As is discussed in the introduction, some aspects of MR whistlers can be qualitatively explained in terms of propaga-

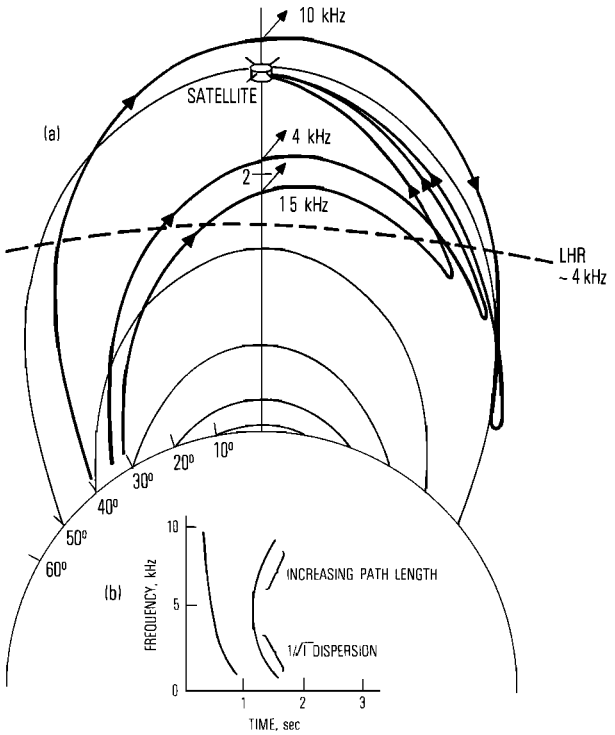

Fig. 2. (*a*) Ray paths for the second component of an MR whistler received at the magnetic equator ($L \sim 2.4$). (*b*) Computed spectra corresponding to the ray paths in Figure 2*a*. The comments on the component refer to the dominant factor determining the time delay for that frequency range.

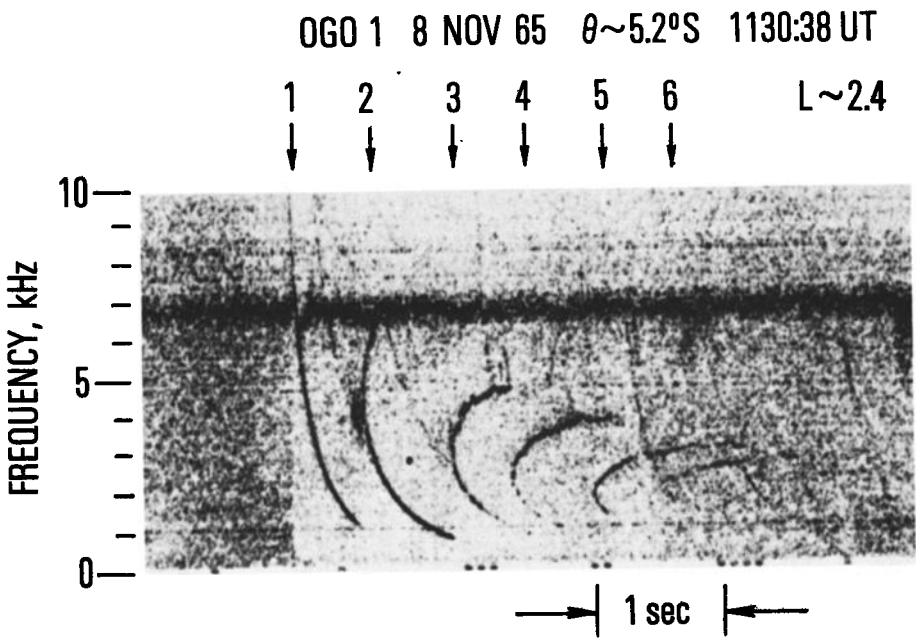

Fig. 3*a*. Frequency-time spectrogram of a typical MR whistler observed near the magnetic equator at $L \sim 2.4$. The dark band at 7 kHz is interference associated with the voltage-controlled oscillator used to indicate amplitudes.

tion through a 'smooth' magnetosphere (i.e., free of sharp electron density perturbations). Utilizing the Stanford ray-tracing computer program [*Walter*, 1969] with a simple diffusive equilibrium magnetospheric density model [*Angerami and Thomas*, 1964] consisting of a mixture of half H^+ and half O^+ at 1000 km, a constant base level density of 1.15×10^4 el/cc at 1000 km, and a uniform temperature of 1200°K, one can fit the general frequency versus time characteristics of the MR whistler spectrogram of Figure 3*a*, as is shown in Figure 3*b*. The calculated and measured time delays show good agreement for the first two components but diverge slightly above 2 kHz for the higher-order traces. Another feature of Figure 3*b* is that the calculated time delays for the traces exhibit no sharp discontinuities at the upper and lower cutoff frequencies of the observed spectra. As shown in Figure 3*b*, the calculated traces extend smoothly well beyond the frequency range of the observed traces.

Simulation of Upper and Lower Cutoffs

Figure 4 shows calculations of frequency versus starting latitude for an MR whistler observed at the typical position of $L \sim 2.4$ on the magnetic equator. The spread of starting latitudes is very small for the first component but approaches 20° for the fifth component, the high-frequency ray paths starting at the higher latitudes. If by some means one restricts the available input latitudes to the range 22°–36° and computes the resultant MR whistler spectrogram, an upper- and lower-frequency cutoff pattern emerges as shown in Figure 5. This pattern is similar to that of the observed whistler in Figure 3*a* except that the first component is missing. From this result one could infer that the observed upper and lower cutoff patterns of MR whistlers are related to some loss mechanism acting on initial excitation of whistler waves in the lower ionosphere. The absence of the first trace is not a serious problem and will be remedied in a later section.

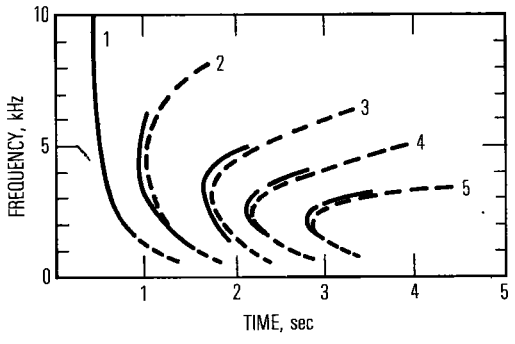

Fig. 3*b*. Comparison of calculated (dashed lines) and measured (solid lines) time delays of the MR whistler frequency-time spectrogram received by Ogo 1 on November 8, 1965.

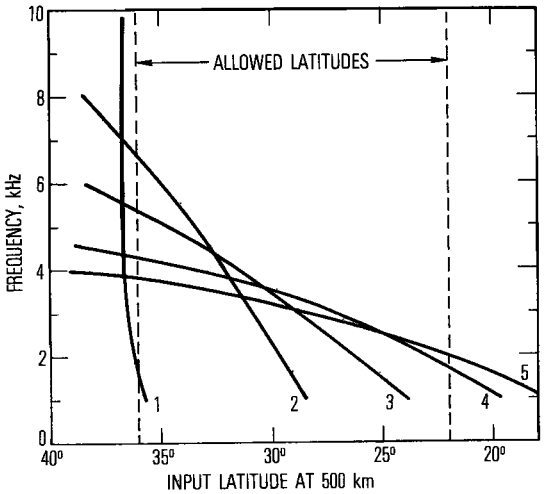

Fig. 4. Excitation latitude at 500 km versus frequency for an MR whistler observed at an equatorial satellite position at $L \sim 2.4$. The number at the bottom of each trace refers to the corresponding MR whistler trace number in Figures 2*a* and 2*b*. These calculations are based upon the 'smooth' magnetospheric density model. The 'allowed latitude' range refers to a heuristic procedure of restricting excitation latitudes which is explained in the text.

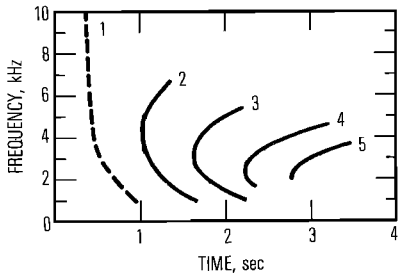

Fig. 5. Calculated MR frequency-time spectrogram corresponding to restricting the input latitudes to the range between 22° and 36° as shown in Figure 4. The missing first component is denoted by dashed trace 1. Notice that the upper- and lower-frequency cutoff patterns closely resemble the cutoff pattern exhibited by the MR whistler spectrogram in Figures 3*a* and 3*b*.

Upper-Frequency Cutoffs

The success (cf. Figure 5) in reproducing sharp upper cutoffs of MR whistlers by artificially restricting VLF input latitudes suggests consideration of a propagation mechanism in the magnetosphere which does the same. An investigation of the effects on MR ray paths of many different magnetospheric density models revealed one model that would restrict the input latitudes of MR whistler ray paths that reach typical magnetospheric observing points. This density model has a sharp cross-L density drop-off located along a particular field line. Figure 6*a* shows calculated MR rays for a density model that includes an abrupt drop-off at $L \sim 2.0$. MR whistler rays which start at or below 32° latitude suffer only a slight bending as they pass through $L \sim 2.0$. However, because of the density drop-off, rays starting between 32° and 42° latitude are 'trapped' at $L \sim 2.0$ in a longitudinal mode similar to that of ducted whistlers. Figure 6*b* shows the same ray paths in Figure 6*a* plotted in dipole latitude–L shell space to emphasize the trapping of whistler rays by the sharp density drop-off at $L \sim$ 2.0. The density model is plotted in Figure 6*c*. These plots demonstrate that the sharp cross-L density drop-off at $L \sim 2.0$ prevents upgoing whistler rays starting between 32° and 42° latitude from contributing to MR whistlers.

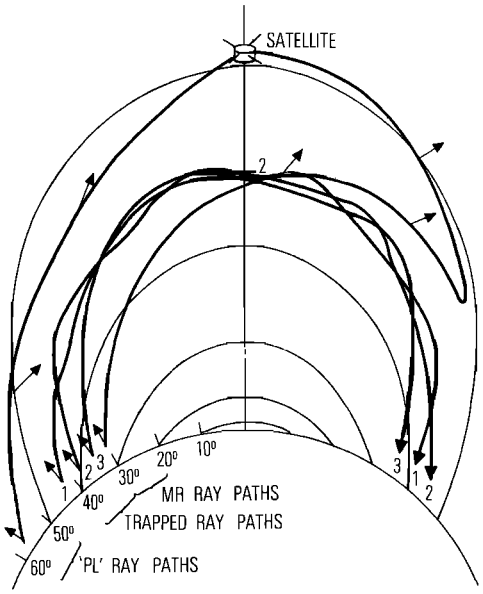

Fig. 6*a*. The trapping of upgoing whistler rays by an abrupt density drop-off at $L \sim 2$. The rays (labeled 1, 2, and 3) excited between 32° and 42° are totally trapped by the irregularity and return to earth in the conjugate hemisphere. A ray starting at 30° eventually propagates into the MR whistler mode without any large ray path perturbations by the density irregularity. The ray starting near 60° is bent inward by a gradual density roll-off between $L \sim 3$ and $L \sim 4$ such that it becomes the source of the first MR whistler trace.

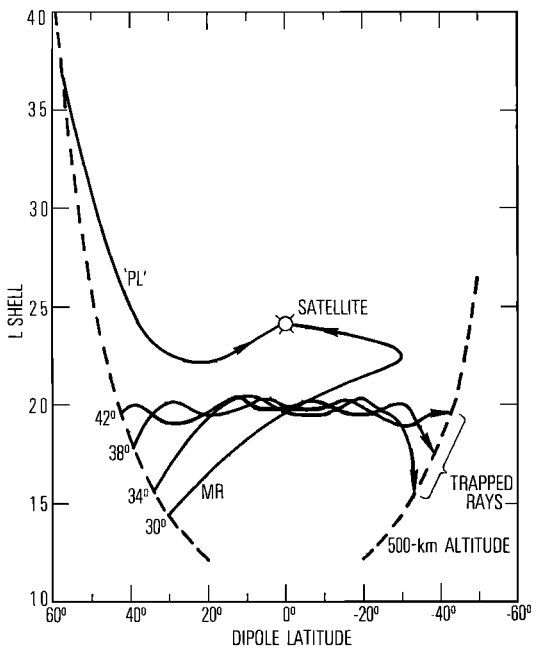

Fig. 6*b*. Trapping of rays as plotted in dipole latitude–L shell space.

The condition for trapping of upgoing nonducted whistler rays is approximately given by

$$\cos \psi_1 > N(L > 2.0)/N(L < 2.0)$$

where ψ_1 is the wave normal angle as the ray initially crosses the density drop-off, $N(L < 2.0)$ is the density inside the density drop-off, and $N(L > 2.0)$ is the density outside the density drop-off.

This condition was adapted from *Smith et al.* [1960], who used it to explain trapping of whistlers by enhancements of ionization. The difference between this case and the one of Smith et al. is that the density drop-offs trap nonducted whistler rays in the magnetosphere, whereas enhancements trap only whistler rays that start inside the field-aligned enhancement or duct. Ray-tracing calculations predict that when $N(L > 2.0)/N(L < 2.0) < 0.66$, complete trapping occurs, but for higher values of the ratio the rays are only partially trapped and eventually go into the MR mode. Complete trapping only

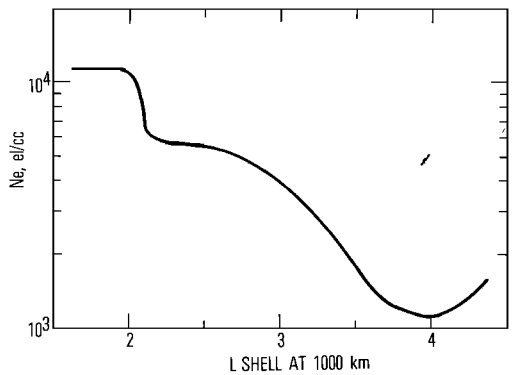

Fig. 6*c*. The density model for the ray path calculations of Figures 6*a* and 6*b* plotted in L shell coordinates at 1000 km.

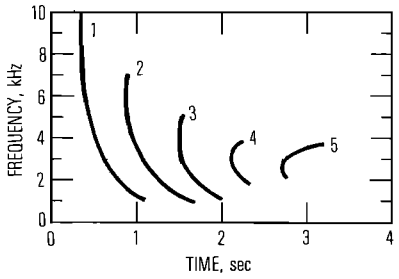

Fig. 7. Calculated MR spectrogram with a restored first component based upon the ray paths and density model of Figure 6.

occurs if the gradient of the refractive index [*Scarabucci*, 1969] is dominated by the density gradient contribution; otherwise, the magnetic field 'curvature' contribution will predominate.

When a ray with a wave normal angle less than ψ_1 crosses the abrupt density drop-off, the direction of rotation of the wave normal will be changed due to the density gradient. (The reader is referred to *Smith et al.* [1960] for the details of a Snell's law explanation of the rotation of the wave normal.) The reversal of the wave normal rotation causes the ray path to reverse direction such that the ray crosses back into the region where the magnetic field 'curvature' dominates. The wave normal again changes direction of rotation, and the ray propagates back to the density drop-off, where the process repeats. Thus the ray oscillates about the field line of the drop-off until it reaches the ionosphere in the opposite hemisphere.

Restoration of the First MR Component

In an earlier section of this paper we discussed restricting the excitation latitudes to the range 36°–22°. This procedure artificially eliminated the first component from a calculated MR spectrogram. Insertion of a sharp density drop-off at $L \sim 2$ achieves the same result. The first component may be restored by the following argument. If we insert into the electron density model a roll-off of density between L values of 3 and 4, we can cause a pronounced bending of calculated ray paths starting between latitudes of 50° and 60°. For this case our smoothed density roll-off model is based upon H^+ ion data as measured at 1000 km by Ogo 2 [*Taylor et al.*, 1968]. These ray paths cross the equator between $L \sim 2$ and $L \sim 3$ at the same time delay as would be calculated for the first component in Figure 1*b*. This mode was first discovered by *Scarabucci* [1969], who called it the prolongitudinal (PL) mode.

This interpretation of the origin of the first MR component has many implications about the observations of fractional hop whistlers on the same Ogo 1 pass of Figure 3*a*. Many fractional hop whistlers were observed without MR components, but conversely, no MR whistlers were observed without a first component. This observation implies that the MR atmospheric sources were located in the mid-latitudes ($60° < \theta < 30°$), since sources at those latitudes could excite both the PL and the MR whistler modes. The atmospheric sources for the fraction hop whistlers were probably at latitudes greater than 60°, since wave guide attenuation would prevent the lower-latitude MR modes from being excited.

Comparison of the Two Methods for Modeling the Upper-Frequency Cutoffs

The heuristic method of achieving an upper-frequency cutoff on MR whistlers by restricting the input latitudes predicts that trapping must occur for input latitudes greater than 36°.

TABLE 1. Defocusing Loss in Decibels

Frequency, kHz	$N = 2$	$N = 3$	$N = 4$	$N = 5$
5	9.0	5.8	...	.
4	9.5	7.5	5.0	3.0
3	9.6	8.2	6.9	5.4
1	10.0	8.8	7.6	6.2

Here N is the component number.

The MR whistler spectrogram as shown in Figure 7 resulting from ray tracing in a model magnetosphere with a density drop-off at $L \sim 2$ shows that one can achieve the same cutoff pattern as the earlier result except that trapping occurs above latitudes of 32°. The discrepancy between the two results may be cleared up by noting that the density drop-off does slightly modify the MR ray paths that pass through it. The distorted ray paths pass through slightly higher L shells than do ray paths in a 'smooth magnetosphere' which was the basis of the heuristic method. Thus while the latitude above which trapping occurs is model dependent, the concept of MR whistler upper-frequency cutoffs being produced by trapping of upgoing whistler rays appears to remain valid.

Other Experimental Evidence

The presence of such sharp density drop-offs in the top side ionosphere has been confirmed by *Taylor et al.* [1971], who measured very sharp drop-offs in H^+ density at $L \sim 1.8$ and $L \sim 2.7$ after a magnetic storm ($Kp_{max} = 5$). *Grebowsky et al.* [1970] reported coincident top side and magnetospheric H^+ density measurements which indicate that this density structure may persist in the magnetosphere well after a magnetic storm has subsided. These measurements show a typical quiet top side profile similar to the smooth profile of *Taylor et al.* [1971] taken a day after the storm. But the magnetospheric H^+ density profile of *Grebowsky et al.* [1970] contains sharp cross-L density drop-offs at $L \sim 1.7$, $L \sim 2.6$, and $L \sim 3.5$. Thus the top side H^+ profile may not indicate the true density structure of the magnetosphere.

Similar persistent sharp drop-offs in electron density have also been observed by *Bewersdorff and Sagalyn* [1972] in the region $L \sim 2$–3. These density irregularities seem to remain for several days after a magnetic storm and appear to be sharp enough to trap upgoing nonducted whistler rays.

Low-Frequency Cutoffs

There are three loss mechanisms operating on the low-frequency (below the nose) portions of MR whistlers: wave guide attenuation, D region absorption, and defocusing of MR ray paths. We will examine the latter two mechanisms first.

Calculations of D region absorption loss [*Helliwell*, 1965] show that for a vertically incident wave at 2 kHz in a nighttime ionosphere the attenuation increases from 4 dB at 30° latitude to 10 dB at 20° latitude. Since one generally does not observe

TABLE 2. Wave Guide Attenuation in Decibels for an Atmospheric Source Location at 40° Magnetic Latitude

Frequency, kHz	$N = 3$	$N = 4$	$N = 5$
4	17.0	14.0	.
3	22.0	26.0	22.0
2	27.8	33.6	34.8
1	32.0	41.0	44.0

Here N is the component number.

TABLE 3. Total Attenuation in Decibels for an Atmospheric Source Location at 40° Magnetic Latitude

Frequency, kHz	$N = 3$	$N = 4$	$N = 5$
4	28.1	22.4	...
3	34.4	37.8	31.6
2	41.5	47.8	48.2
1	47.3	60.6	67.4

Here N is the component number.

TABLE 4. Total Attenuation in Decibels for an Atmospheric Source Location at 25° Magnetic Latitude

Frequency, kHz	$N = 3$	$N = 4$	$N = 5$
5	29.3	...	...
4	24.1	22.5	...
3	20.4	17.9	17.6
2	15.3	17.3	18.2
1	17.3	30.5	37.4

Here N is the component number.

MR frequency components which enter the ionosphere below ~20°, D region absorption is certainly one loss mechanism which follows the observations.

Another loss mechanism is the defocusing loss suffered by a tube of rays which arrives at the satellite. The defocusing loss can be determined by taking the ratio of the input (at 500 km) and output (at the satellite) cross-sectional areas of this tube of rays. On the assumption that the rays remain in the same magnetic meridian the defocusing loss can be expressed as

$$\text{loss (dB)} = 10 \log_{10} [(d_2/d_1)(r_2/r_1)]$$

where d_1, d_2 are separations between two adjacent rays at input altitude and at the satellite, respectively, and r_1, r_2 are perpendicular distances from the geomagnetic dipole axis to the input point and to the satellite point, respectively.

The defocusing loss for the case of Figures 4 and 5 is given for several frequencies in Table 1. For the higher-order components the low frequencies undergo more defocusing than the frequencies above the nose, an effect which supplements the D region absorption mentioned above. The minimal defocusing of the upper frequencies, e.g., the fifth component, may partially account for their enhanced appearance on the spectrogram of Figure 3*a*. The total low-frequency loss due to defocusing and absorption may be greater than 10 dB in comparison with that of frequencies above the nose.

Since energy from an atmospheric source must travel over a wide range of latitudes to excite MR whistlers, another important loss mechanism is earth-ionosphere wave guide attenuation. According to a review paper by *Maxwell* [1967] the propagation attenuation coefficient peaks in the 1- to 5-kHz region at a mean figure of ~20 dB per 1000 km. This figure corresponds to ~2 dB per degree of magnetic latitude. For the purpose of calculating typical attenuation values we can assume an atmospheric source location of 40° magnetic latitude for the MR whistler of Figure 3*a*. The wave guide attenuation can then be calculated by using Figure 4 and the mean attenuation coefficient. The results are given in Table 2. Not unexpectedly, the low frequencies (1 kHz) are highly attenuated (40 dB) because of their long path lengths in the wave guide.

If we now add all attenuation rates (wave guide, spreading, and D region absorption) to obtain a total attenuation rate, we arrive at Table 3. This table predicts a 30- to 40-dB difference between the amplitudes of frequency components well above the nose and well below the nose on traces 3, 4, and 5. Studies of noise amplitudes observed on the Ogo 4 VLF receiver (similar to that on Ogo 1) [*Muzzio and Angerami*, 1972] yield a 40-dB dynamic range for the spectrogram-VLF receiver–satellite telemetry system. This 40-dB dynamic range is comparable to the 30- to 40-dB attenuation range calculated for a typical MR component. Thus if the receiver AGC adjusts to the strongest frequency component above the nose, the low frequencies will be in the background noise. Such is the case for traces 3 and 4.

Traces 5 and 6 display a different type of low-frequency cutoff characteristic than that of traces 3 and 4. Their cutoffs are rather abrupt and are very similar to the type of cutoff

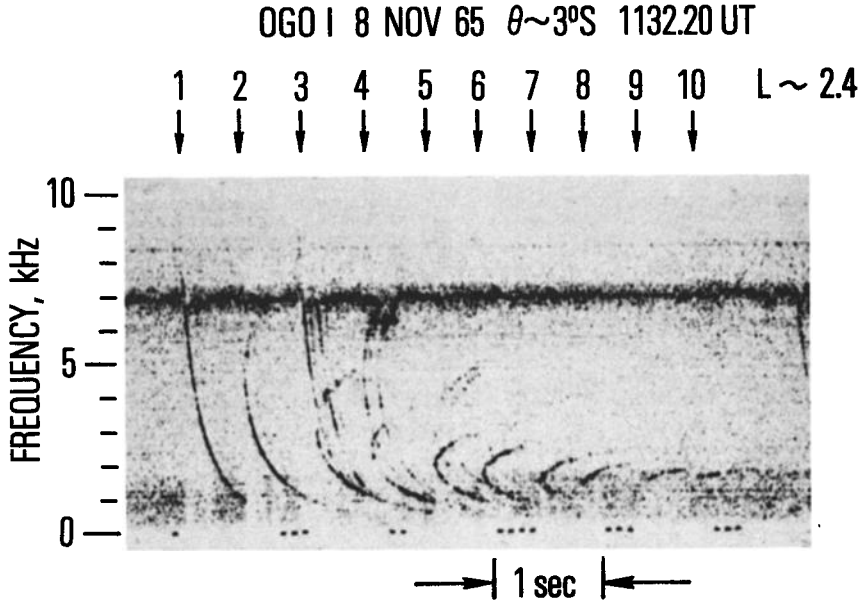

Fig. 8. Frequency-time spectrogram of an MR whistler with 10 components with well-defined upper- and lower-frequency cutoff patterns.

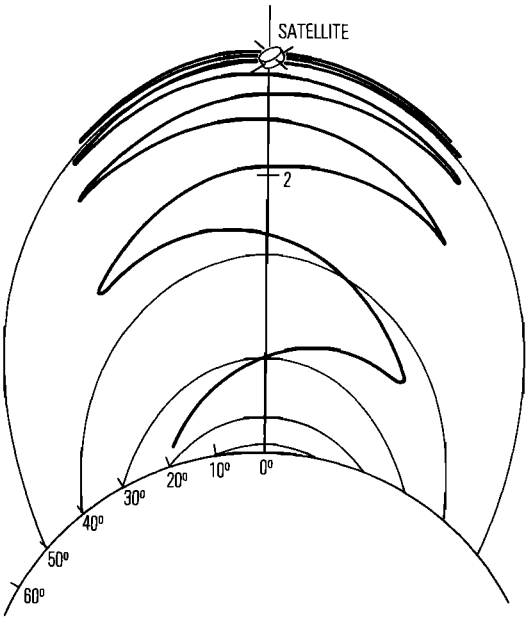

Fig. 9. Calculated ray path for 1.75 kHz starting at 18°. The satellite location allows it to observe the higher-order MR ray paths.

predicted by artificially limiting excitation latitude. This similarity suggests that the large values of attenuation for the low frequencies produce an 'effective range' for an atmospheric source in the earth-ionosphere wave guide. If the excitation latitude is lower than the extent of the effective range, the particular component is not observed at the satellite.

The effect of moving the lowest excitation latitude down to 18° magnetic latitude is illustrated by Figure 8. This MR whistler was observed on the same satellite pass as the example of Figure 3*a*. The large number of components (10) is a rare occurrence mainly because of the wave guide attenuation effect. The upper portions (above the nose) of traces 2, 3, and 4 are reduced in signal strength in comparison with the same traces in Figure 3*a*. An atmospheric source location at ~25° would produce such an effect and would also allow energy to propagate down to 18°. Table 4 lists the attenuation rates for this source location and shows a different attenuation pattern from that of Table 3. The frequency region about and below the nose shows the least amount of attenuation. One does not also observe the large range (40 dB) of attenuation rates in Table 4.

The satellite was also at the optimum point to observe the large number of MR rays, as illustrated by Figure 9. Above $L_{eq} \sim 2.3$ the local LHR frequency is lower than the signal frequency of 1.75 kHz, and the ray paths tend to be closely field-aligned. Most of the higher-order MR whistler components are excited in the 18°–20° latitude region.

Discussion and Conclusions

Thorne [1968] hypothesized a secondary peak in the electron energy distribution near 10 keV which would allow Landau resonant particle interactions with MR whistler waves, although *Bernard* [1973] has shown that alternative cyclotron interactions would also work. His approach used Landau growth and damping to explain quantitatively the upper- and lower-frequency cutoffs as well as the enhanced signal strengths. However, this paper suggests that several such features of observed MR whistler spectra can be explained by propagation in a cold plasma without the need of hot plasma particles. Landau and cyclotron particle interactions may be present, but more quantitative work is needed to evaluate their importance.

This paper has shown that the general characteristics of MR whistler frequency-time spectrograms can be successfully explained by VLF ray-tracing calculations utilizing simple ion and electron density models of the magnetosphere. Observed departures of MR spectra from predictions based on smooth models can then be used to model magnetospheric density structure. The results of this investigation of MR whistler cutoffs have implied the existence of sharp cross-L density drop-offs in the magnetosphere. A future paper will examine in detail this magnetospheric density structure and its relation to MR whistlers and magnetic storms.

Acknowledgments. The author wishes to thank R. A. Helliwell, D. L. Carpenter, J. J. Angerami, and R. L. Smith for their guidance and advice during the course of the development of this topic. This research was supported by NASA contract NGL-05-020-008. The author also acknowledges the support of U.S. Air Force Space and Missile Systems Organization contract F04701-74-C-0075 while he was at the Aerospace Corporation. The major part of this research was carried out while the author was at the Radio Science Laboratory, Stanford University, Stanford, California.

The Editor thanks R. E. Barrington and S. D. Shawhan for their assistance in evaluating this paper.

References

Angerami, J. J., and J. O. Thomas, Studies of planetary atmosphere, 1, The distribution of electrons and ions in the earth's exosphere, *J. Geophys. Res., 69,* 4537, 1964.

Bernard, L. C., Amplitude variations of whistler-mode signals caused by their interaction with energetic electrons of the magnetosphere, Ph.D. dissertation, Stanford Univ., Stanford, Calif., Dec. 1973.

Bewersdorff, A. B., and R. C. Sagalyn, Spatial and temporal variations of the thermal plasma between 3000 and 5700 km at $L = 2$ to 4, *J. Geophys. Res., 77,* 4734, 1972.

Edgar, B. C., The structure of the magnetosphere as deduced from magnetospherically reflected whistlers, Ph.D. dissertation, Stanford Univ., Stanford, Calif., April 1972.

Grebowsky, J. M., N. K. Rahman, and H. A. Taylor, Jr., Comparison of coincident Ogo 3 and Ogo 4 hydrogen ion composition measurements, *Planet. Space Sci., 18,* 965, 1970.

Helliwell, R. A., *Whistlers and Related Ionospheric Phenomena,* Stanford University Press, Stanford, Calif., 1965.

Kimura, I., Effects of ions on whistler-mode ray tracing, *Radio Sci., 1,* 269, 1966.

Maxwell, E. L., Atmospheric noise from 20 Hz to 30 kHz, *Radio Sci., 2,* 637, 1967.

Muzzio, J. L. R., and J. J. Angerami, Ogo 4 observations of extremely low frequency hiss, *J. Geophys. Res., 77,* 1157, 1972.

Scarabucci, R. R., Interpretation of VLF signals observed on the Ogo-4 satellite, Ph.D. dissertation, Stanford Univ., Stanford, Calif., Oct. 1969.

Smith, R. L., and J. J. Angerami, Magnetospheric properties deduced from Ogo 1 observations of ducted and nonducted whistlers, *J. Geophys. Res., 73,* 1, 1968.

Smith, R. L., R. A. Helliwell, and I. W. Yabroff, A theory of trapping of whistlers in field-aligned columns of enhanced ionization, *J. Geophys. Res., 65,* 815, 1960.

Taylor, H. A., Jr., H. C. Brinton, M. W. Pharo III, and N. K. Rahman, Thermal ions in the exosphere: Evidence of solar and geomagnetic control, *J. Geophys. Res., 73,* 5521, 1968.

Taylor, H. A., Jr., J. M. Grebowsky, and W. J. Walsh, Structured variations of the plasmapause: Evidence of a corotating plasma tail, *J. Geophys. Res., 76,* 6806, 1971.

Thorne, R. M., Unducted whistler evidence for a secondary peak in the electron energy spectrum near 10 keV, *J. Geophys. Res., 73,* 4895, 1968.

Walter, F., Nonducted VLF propagation in the magnetosphere, Ph.D. dissertation, Stanford Univ., Stanford, Calif., Oct. 1969.

(Received February 24, 1975;
accepted July 14, 1975.)